Renewable Energy 172 (2021) 697–713

Contents lists available at ScienceDirect

Renewable Energy

journal homepage: www.elsevier.com/locate/renene

Combining methodologies on the impact of inter and intra-annual variation of wave energy on selection of suitable location and technology

Bahareh Kamranzad [a, b, *], Pengzhi Lin [c], Gregorio Iglesias [d, e]

[a] Graduate School of Advanced Integrated Studies in Human Survivability (GSAIS), Kyoto University, Yoshida-Nakaadachi 1, Sakyo-ku, Kyoto, 606-8306, Japan
[b] Hakubi Center for Advanced Research, Kyoto University, Yoshida Honmachi, Sakyo-ku, 606-8501, Kyoto, Japan
[c] State Key Laboratory of Hydraulics and Mountain River Engineering, Sichuan University, 24, South Section No.1, Yihuan Road, Chengdu, 610065, PR China
[d] MaREI, Environmental Research Institute & School of Engineering, University College Cork, College Road, Cork, Ireland
[e] School of Engineering, University of Plymouth, Plymouth, PL4 8AA, United Kingdom

ARTICLE INFO

Article history:
Received 26 November 2020
Received in revised form
2 March 2021
Accepted 12 March 2021
Available online 18 March 2021

Keywords:
Wave energy
Southern China
Sustainability index
WEI
MCA factor

ABSTRACT

In this study, based on 55 years' worth of high-resolution simulated wave data using numerical modeling off the southern coasts of China, intra-annual and decadal variations of the wave climate and wave energy were evaluated. The results show that it is important to consider a sufficiently long time period for wave energy assessment to take into account the changing climate. The high-resolution wave dataset enabled the quantitative analysis in both nearshore and offshore, and the quantitative analysis was performed in two phases: First, using two different approaches. i.e., "Climate-dependent Sustainability Index" and "Wave Exploitability Index", the wave power and its short and long-term changes were considered to prioritize the candidate stations for further assessment. Then, a modified "Multi-Criteria Approach" consisting of both sea state and Wave Energy Converters (WECs) was applied to determine the most suitable combination of WEC and location in the domain, which is Wave Dragon in the eastern parts of the domain with the energy production of around 92,000 MWh for a single device. The results provide the quantitative analysis for different scenarios of development plans in the study area on the selection of appropriate location and technology.

1. Introduction

The usage of renewable energies as an alternative to fossil fuels is growing to adjust the consequences of global warming and prevent the energy crisis which will occur soon after the termination of fossil resources [1]. Interestingly, despite the COVID-19 crisis in 2020, renewable power is still growing strongly, and renewable electricity generation will increase by 7% in 2020 [2]. Although wind and solar are leading sources of renewable energies, the exploitation of the vast resources of ocean energies is still under development, and may well supply in the future a considerable part of the energy demand in many countries. Ocean wave energy, a predictable and endless source of energy with the highest density among all renewables and low visual and environmental impacts, has additional advantages such as broad geographic viability, conservation of terrestrial resources, and adding to the diversity of the renewable energy mix [3,4]. In addition to power generation, wave energy technologies can be used for other purposes such as desalination, hydrogen production, pumping and heating processes [3], and coastal protection [5,6].

China, with considerable efforts in developing renewables, has announced the target for reaching net-zero emissions by 2060 [2]. Vicinity to East and South China Sea and settlement of large populations in coastal cities highlights the importance of using ocean renewables in development plans for China. In order to achieve this purpose, extensive research has been carried out on the assessment of available ocean resources and especially the wave energy to investigate the available resources based on various sources of data, and considering different time spans for the analysis (e.g.

* Corresponding author. Graduate School of Advanced Integrated Studies in Human Survivability (GSAIS), Kyoto University, Yoshida-Nakaadachi 1, Sakyo-ku, Kyoto, 606-8306, Japan.
E-mail address: kamranzad.bahareh.3m@kyoto-u.ac.jp (B. Kamranzad).

https://doi.org/10.1016/j.renene.2021.03.062

Refs. [3,7–24]). However, recent studies have shown that as well as the amount of energy and its seasonality, considering the changing climate, which may affect the available resources in the long-term, is necessary [6,25–35]. Hence, in a previous study [36], the authors estimated the wave energy potential, its short-term variation and long-term change for 55 years in the South China Sea based on simulated wave data and found that the long-term change has been considerable in the areas with the highest wave energy potential. Hence it is necessary to consider the impact of changing climate when selecting the potential locations for future development. They also showed that available resources vary in various decades. Hence, it is important to consider a suitable time span and preferably long enough to reduce the uncertainties in the estimation of the resources.

In this study, the outcomes of the previous study are utilized to perform a higher resolution wave modeling and estimation of wave energy in the areas with least intra-annual variation and long-term change, i.e., mainly off the southern coasts of China. The high-resolution wave model employs the boundary condition from a previous work [36] and long-term wind dataset of 55 years to generate the wave characteristics in the study area for estimation of wave resources with higher accuracy. In addition, the quantitative analysis is done for selected stations based on a high-resolution wave dataset to introduce the candidate station using two different methods and discusses different approaches for the first time. The wave dataset in candidate stations is then utilized to estimate various criteria that affect the selection of suitable locations and suitable technologies. Finally, different criteria were combined in a modified factor to define the suitable combination of location/WEC and their energy production.

2. Material and methods

2.1. Study area and data sources

As mentioned in the introduction, previous research done by the authors [36] showed that the northern parts of the South China Sea are suitable for further investigation of wave resources. In this study, a high-resolution model covering the northern parts of the South China Sea and parts of the East China Sea (Fig. 1) was developed to generate the wave characteristics in the long-term. The study area includes deep waters of the order of thousand meters in the south and southeastern parts of the domain, and relatively wide continental shelves in the south of China and northeast of Vietnam (Fig. 2). Fig. 2b shows the area with water depth less than 60 m as desirable depth for the installation of most of the WECs [37]. In addition, there are giant sand wave fields called "Taiwan Banks" located between China and Taiwan with heights up to 22.5 m and wavelengths up to 2115 m [38,39] (shown in Fig. 2b).

The wave modeling was carried out using the SWAN (Simulating WAves Nearshore) model Cycle III version 41.31 [40]. The input wind field was JRA-55 model developed by Japan Meteorological Agency (JMA) with 55 years of reanalysis dataset from 1958 to 2012 [41] with spatial resolution of 60 km (around 0.56°) and temporal resolution of 6-hr. The global bathymetry of the General Bathymetric Chart of the Oceans (GEBCO) with 30 arc-sec spatial resolution was used to provide the bottom input for the model. The model was validated against wave buoy observations in three different periods. More details on the model setup and validation are provided in the next sub-section.

2.2. Model setup and validation

The computational domain of the high-resolution wave model covering the northern waters of the South China Sea (called "KU_SC" hereafter) includes the longitudes of 105.5 °E–123.5 °E and latitudes of 17 °N – 30 °N (Fig. 1). The spatial and temporal resolutions of the computational grid are 0.1 ° × 0.1 ° and 30 min, respectively. The boundary conditions were obtained from the parent model covering the South China Sea and parts of the East China Sea ("KU_SCS") forced by the same wind field. The parent model has been validated against satellite data [36]. The directional computational grid was divided into 36 bins of 10°, and the frequency range (between 0.03 and 1 Hz) was divided into 36 bins on a logarithmic scale. The outputs were generated at spatial and temporal resolutions of 0.1° (in both directions) and 30 min, respectively, in the same area as the computational domain (Fig. 1).

In order to calibrate the model, the outputs were compared with buoy measurements in the middle parts of the domain near Waglan Island located in 114.31 °E and 22.18 °N (Fig. 2). Since Waglan buoy is located in deep water, the calibration of the model was carried out by tuning the whitecapping coefficient, and the changing parameters relevant to friction and breaking were not influential. The calibration of the model was done in order to generate the least error compared with the measurements for three different periods, i.e., 1996/3/8-1996-5-31 (Period-1), 1997/9/15–1997/10/16 (Period-2), and 1999/1/25–1999/2/26 (Period-3). After several trials for calibration, a value of 2.65e-5 was selected for the coefficient for determining the rate of whitecapping dissipation (cds2).

Figs. 3–5 show the time series of significant wave height (H_s), mean wave period (T_m), and wave power (P) for the three calibration periods. The wave power was calculated based on the deep-water approximation formula ($P = 0.49H_s^2T_e$), in which T_e is the energy period, defined by $T_e = m_{-1}/m_0$. For quantitative assessment of the model performance, the error indices, including *Bias*, Root Mean Square Error (*RMSE*), and Scatter Index (*SI*) (Table 1) were calculated according to the following equations:

$$Bias = \overline{y} - \overline{x} \tag{1}$$

$$RMSE = \sqrt{\frac{\sum_i (x_i - y_i)^2}{n}} \tag{2}$$

$$SI = \frac{RMSE}{\overline{x}} \tag{3}$$

where x_i and y_i represent the measured and modeled values at time step i, $\overline{x}$ and $\overline{y}$ are their average values, respectively, and n shows the number of data points. It should be noticed that the calibration of the model has been done in order to minimize *Bias* between the modeled and measured wave power. Table 1 shows that the *Bias* ranges between −0.02 and 0.49 kW/m in different periods of validation.$\overline{\text{Bias}} = y - \overline{x}$

3. Results and discussion

3.1. Intra-annual variability of the wave climate

The validated model was utilized to generate the wave characteristics for 55 years of available data. The long-term dataset was used for calculating the intra-annual variability of wave climate and wave energy. Fig. 6 shows the mean annual H_s, T_e, and P for the entire computational domain, and for the areas with depths below

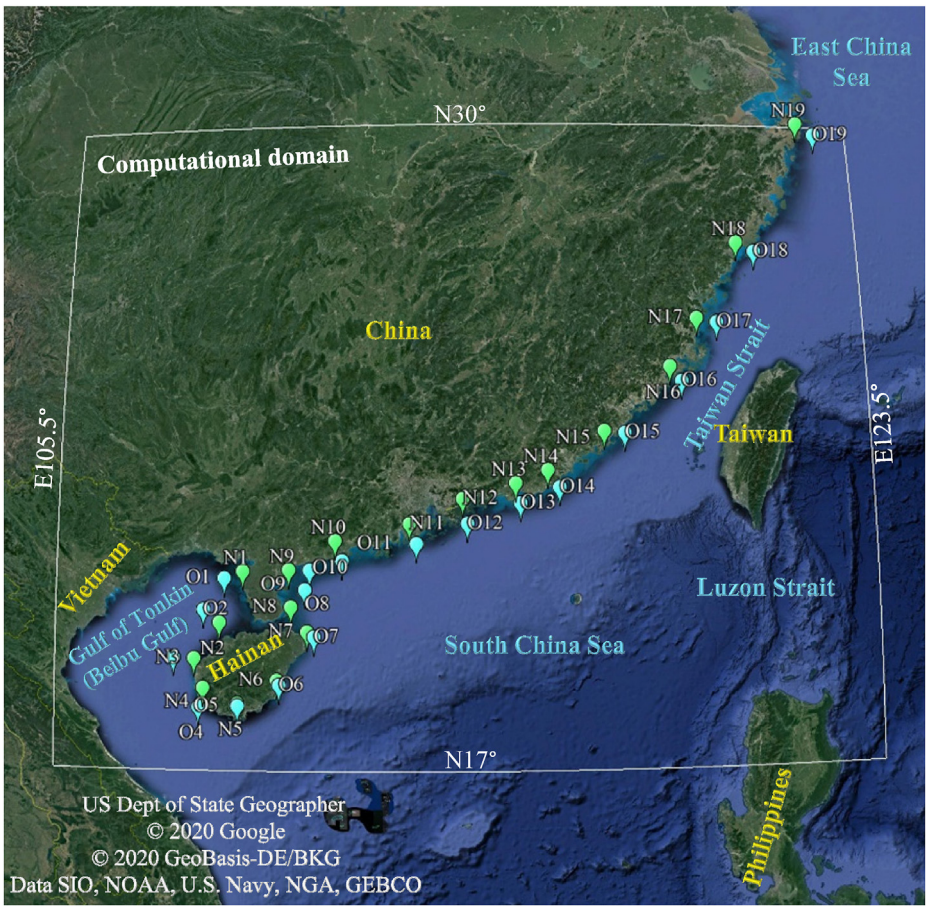

Fig. 1. Study area, computational domain, and location of selected stations.

60 m. According to this figure, the annual mean wave height, energy period, and wave power are the highest off the east of Taiwan and the Philippines due to the vicinity to open ocean. However, the continental shelf in these areas is narrow.

At the other extreme of the energy range, the wave climate in the Gulf of Tonkin (Beibu Gulf) presents the lowest wave heights and periods and, therefore, the least energetic waves. Since the prevailing waves are from the east, the island of Taiwan acts as a natural barrier and reduces the wave power reaching the Chinese coastlines in the Taiwan Strait. The highest wave height along China's coastlines occurs in the east of the domain, in the area not sheltered by Taiwan, while the wave period is highest in both the eastern and central parts of China's coastlines, due to the ocean swells passing north and south of Taiwan, respectively [36]. Consistent with these trends, the wave power in areas with depths below 60 m is highest in the eastern coasts of China and reduces toward the west.

Figs. 7–9 show the seasonal variation of H_s, T_e, and P, respectively. The seasonal Hs varies between 1.8 and 2.8 m, with the highest and lowest values in winter and summer, respectively. The prevailing wave direction also changes from the northeast in winter and spring to the southeast and east-southeast in summer and autumn, respectively. Consequently, the wave climate on the southern coasts of China is mainly affected by swells traveling from the Pacific Ocean during winter and spring and by waves propagating from the southern parts of the South China Sea during summer. In autumn, it is affected by waves from both the Pacific Ocean and the southern parts of the South China Sea.

The energy period reaches its maximum values in autumn, especially in the eastern parts of the domain (Fig. 8). However, the seasonal fluctuation of T_e is lower compared to H_s. According to Fig. 9, the highest mean annual wave power – in the east of the domain – varies between around 20 kW/m in summer and 38 kW/m in winter, which implies a variation of about 90%. The variation in wave power in the middle parts of the southern coasts of China ranges from around 5 kW/m in summer to 15 kW/m in winter. The Gulf of Tonkin experiences the lowest wave power, less than 5 kW/m almost all year round.

3.2. Decadal changes

As well as by intra-annual variations, the wave climate may be affected by long-term changes. A time span of 20–30 years is often considered for wave energy assessment. However, considering the changing climate due to global warming or natural fluctuations, it is important to select the appropriate period for the evaluation of the wave resources and potential, as well as suitable locations for the installation of wave farms. In this study, the access to five decades of wave data enables the investigation of change of wave climate in the long-term, and the comparison of the estimated resources in various time-spans. For this purpose, the mean decadal wave power was calculated for various decades from 1961 to 2010 (Fig. 10). According to this figure, the highest mean decadal wave power has changed from around 30 kW/m during the 1960s to around 20 kW/m in the 2000s, which represents a reduction of about 33% at the hotspots (Luzon Strait). The wave power seems to be more stable during the long-term in the west of Taiwan, south of China, and the Gulf of Tonkin. These results indicate the importance of selecting

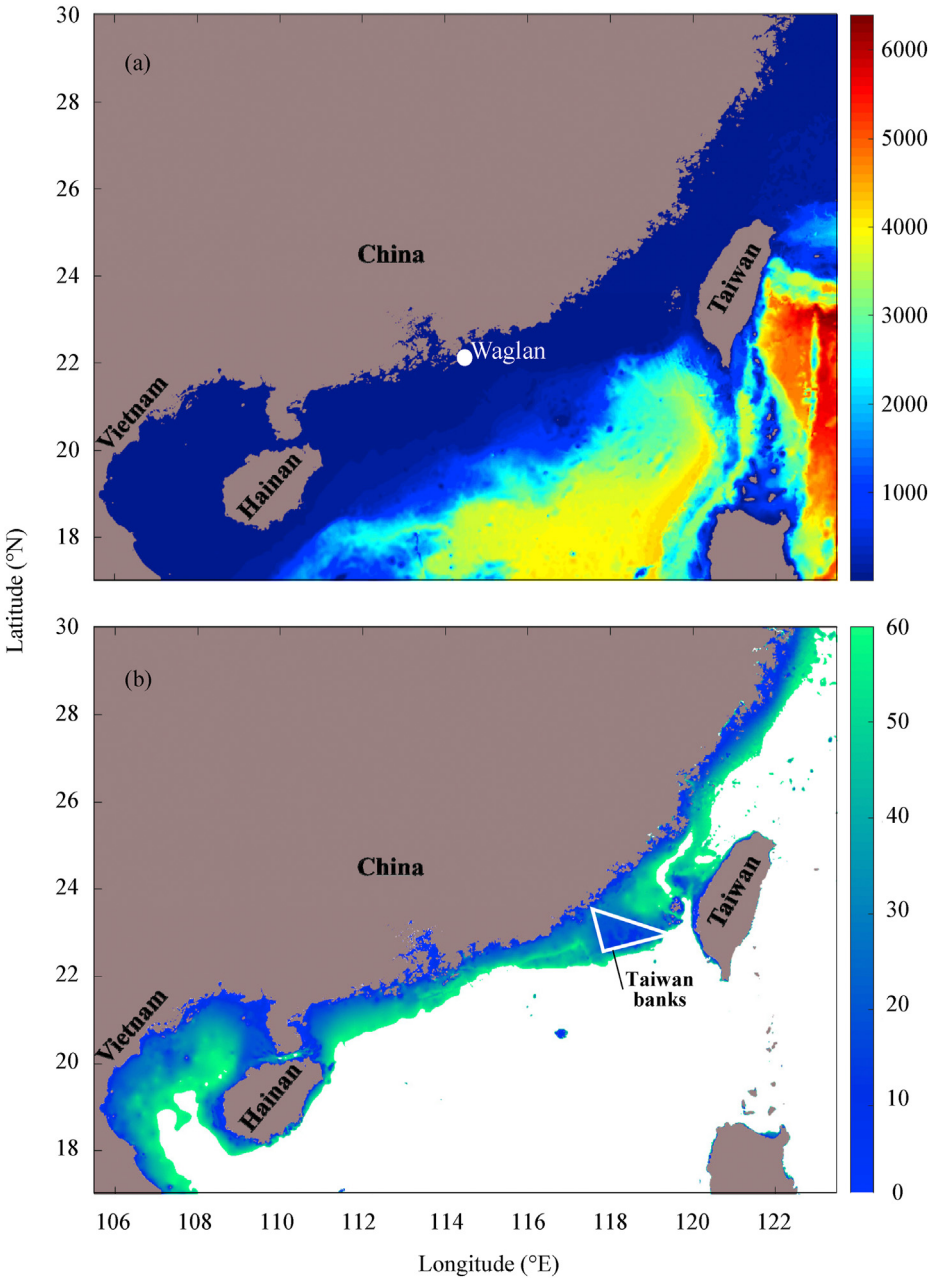

Fig. 2. Bathymetry of study area (depths in m): (a) entire computational domain, and (b) areas with depth below 60 m.

the right time span for analysis of the wave energy resources and emphasizes the necessity of a long-term dataset for considering the impacts of a changing climate and reducing the uncertainties.

3.3. Wave resources and sustainability at selected stations

The previous section showed that the eastern parts of the domain, i.e., the Pacific side of Taiwan and the Philippines, present the largest resources but also significant seasonal variability and considerable long-term change. On this basis, for further investigation and quantitative assessment of the wave energy and available resources, 38 stations (19 nearshore and 19 offshore, Fig. 1) were considered in the northern part of the domain (south and eastern coasts of China), where the wave energy is more stable both in the short and long term. The selection criteria for nearshore stations were: (i) existence of output grid in the vicinity, (ii) highest value of P relative to adjacent cells, (iii) depth of less than 20 m, and (iv) distance to the coast of less than 4 km. The selection criteria for corresponding offshore stations were: (i) highest P relative to adjacent cells, (ii) depth of between 20 and 60 m, (iii) distance to the coast of less than 50 km, and (iv) location outside Taiwan banks (Fig. 2). The coordinates of the selected stations, their water depths, distances from the coast, wave characteristics are presented in Table 2; the locations of the nearshore stations on local map are shown in Fig. 11.

In order to specify the wave condition in nearshore stations for applying the deep water approximation in calculating the wave power (section 2.2.), the wavelength (L) was obtained for the mean wave climate in nearshore stations based on the transitional water equation [42] and shown in Table 2:

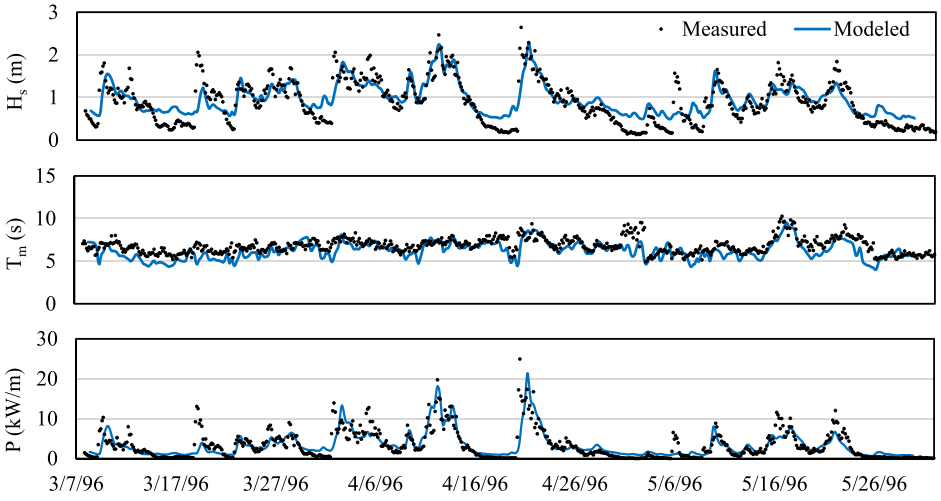

Fig. 3. Time series of modeled and measured H_s, T_m and P (Period-1).

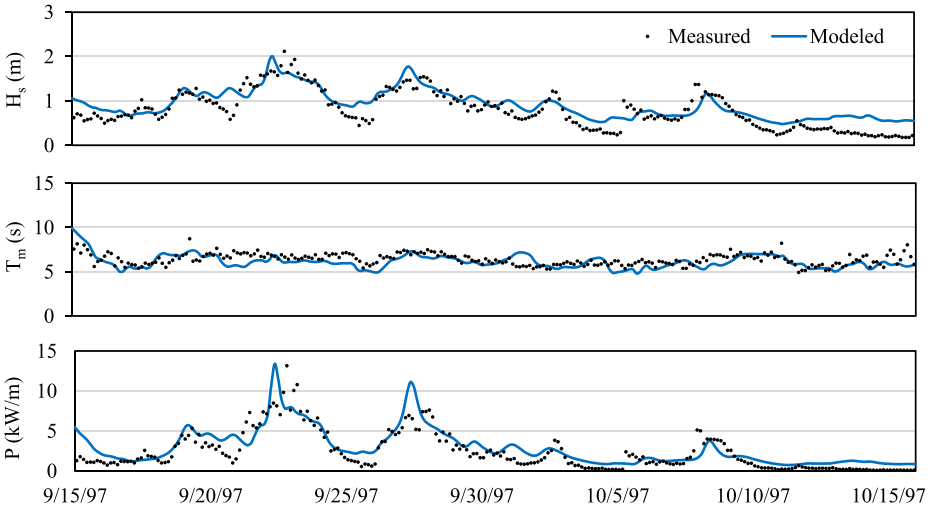

Fig. 4. Time series of modeled and measured H_s, T_m and P (Period-2).

$$L = \left(gT^2/2\pi\right)\tanh(2\pi d/L) \quad (4)$$

in which, T is the wave period, and d is the water depth. According to Table 2, nearshore stations are located in deep or transitional water (with d/L ranging between 0.17 and 0.85), implying that none of them is located in shallow water condition (d/L < 0.05) [42].

For the stations located in transitional water, the wave energy density (E) is calculated as [42]:

$$E = 1/16\rho g H s^2 \quad (5)$$

where ρ is the water density and g is the gravitational acceleration. Wave power in transitional water (P_{tr}) can be obtained as:

$$P_{tr} = ECn$$

in which, C shows the wave speed (equal to L/T), and n is the ratio of the wave group speed to wave speed and is obtained as [42]:

$$n = [1 + (4\pi d/L)/(\sinh \cdot 4\pi d/L)]/2 \quad (7)$$

P_{tr} was compared to P (obtained based on deep water approximation) for the stations located in transitional water (Table 3). The error shown in Table 3 has been calculated as (P- P_{tr}) and varies between −0.014 and −0.297 kW/m for the stations located in transitional water. Hence, in this study, instead of calculating the realistic wave power based on transitional water condition which requires calculation of L for all time steps (80356, in this study), the deep water approximation formula was used for all stations (considering the maximum underestimation of 0.297 kW/m for the average wave climate in nearshore stations located in transitional water).

In order to compare the wave resources in selected stations and choose the most appropriate ones for further quantitative assessment of wave energy and suitable technologies, a combined approach involving two recently proposed indices was employed. First, the Climate-dependent Sustainability Index (SI_p) [43] was utilized, which has been defined based on the ideal conditions corresponding to higher mean annual P ($P_{annual\ mean}$), least rate of

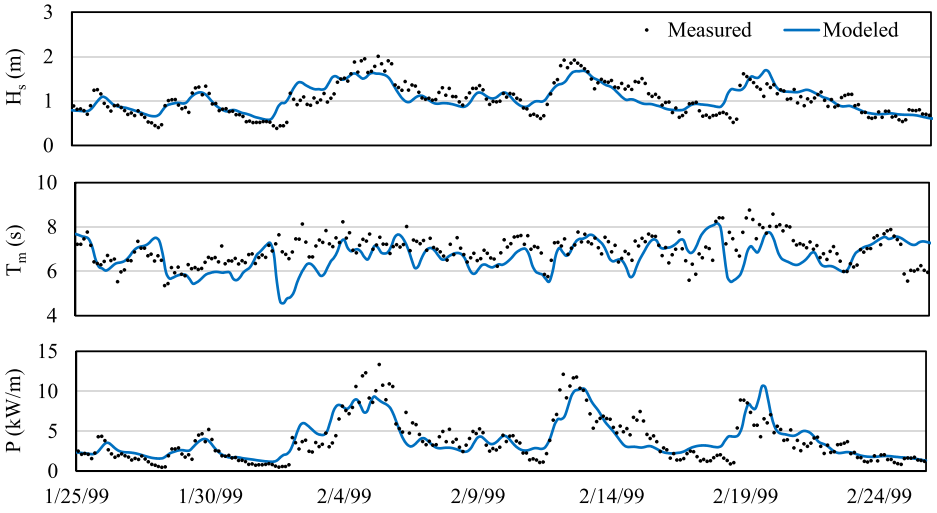

Fig. 5. Time series of modeled and measured H_s, T_m and P (Period-3).

Table 1
Error indices for P, in three periods of validation.

	Bias (kW/m)	*RMSE* (kW/m)	*SI* (%)
Period-1	−0.02	2.08	42
Period-2	0.49	1.37	41
Period-3	0.11	1.57	33

change (RoC) in long-term and least variation in intra-annual scale, i.e., Monthly Variability Index (MVI) [23,44]. RoC is obtained based on the slope of the best linear fit to yearly mean values of P (for 55 years), and MVI is obtained based on the ratio of the difference between the highest and lowest values of mean monthly P to $P_{annual\ mean}$. A cosine function (cos) was used in calculation of RoC to generate the positive output values with the maximum of 1, when the rate of change approaches zero [43].

$$SI_p = \frac{\frac{P_{annual\ mean}}{max(P_{annual\ mean})} \times cos\frac{|RoC|}{max|RoC|}}{MVI} \quad (8)$$

Second, the Wave Exploitability Index (WEI) [26] was used, which is calculated as the ratio of the mean root-mean-square wave height (H_{rms}) to the maximum individual wave height (H_{max}) during the period of simulation:

$$WEI = \frac{\overline{H_{rms}}}{H_{max}} \quad (9)$$

The mean H_{rms} is representative of the mean wave conditions

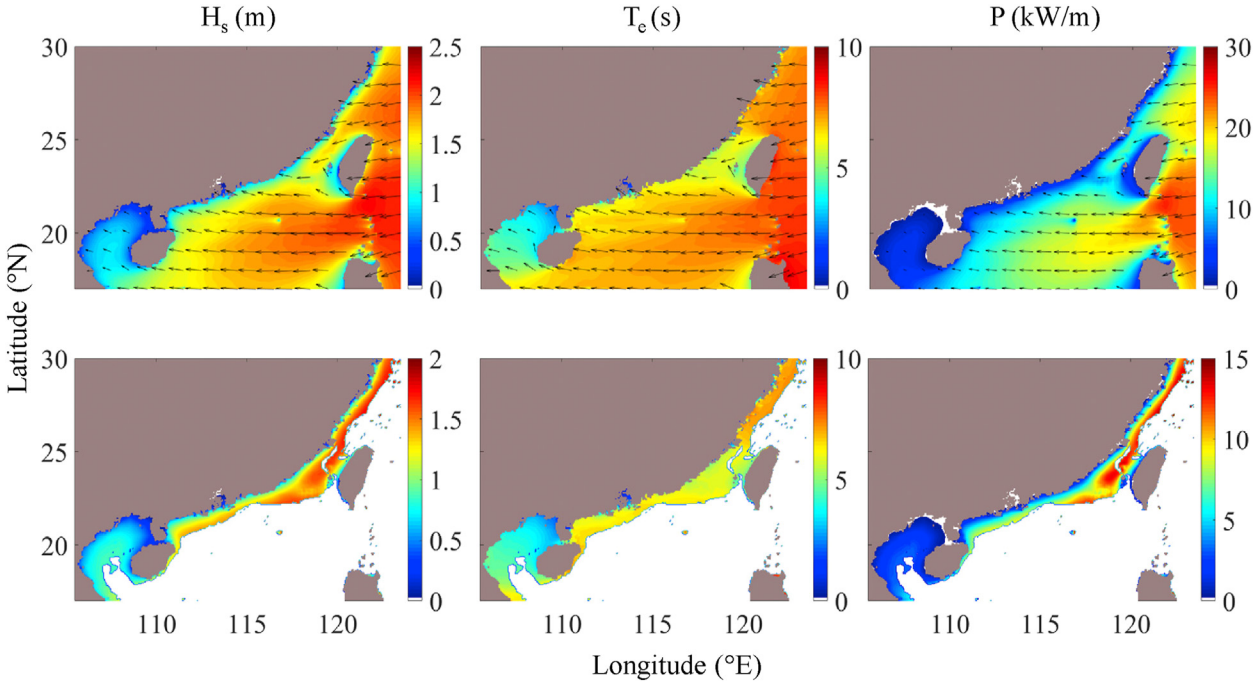

Fig. 6. 55-yearly annual mean values in the entire domain (upper row) and for depths below 60 m (lower row).

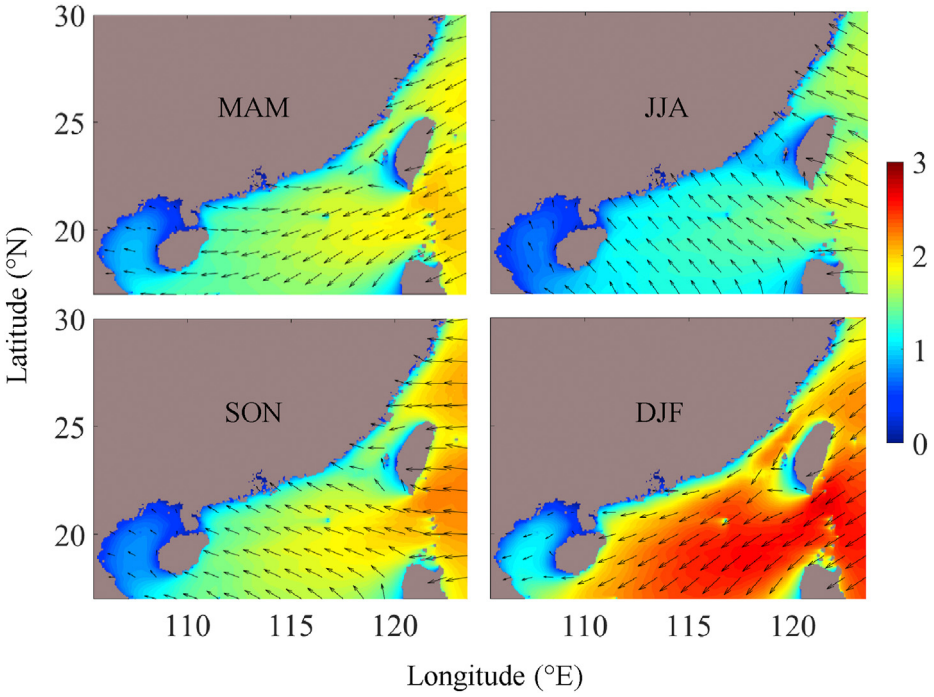

Fig. 7. 55-yearly seasonal mean H_s (m).

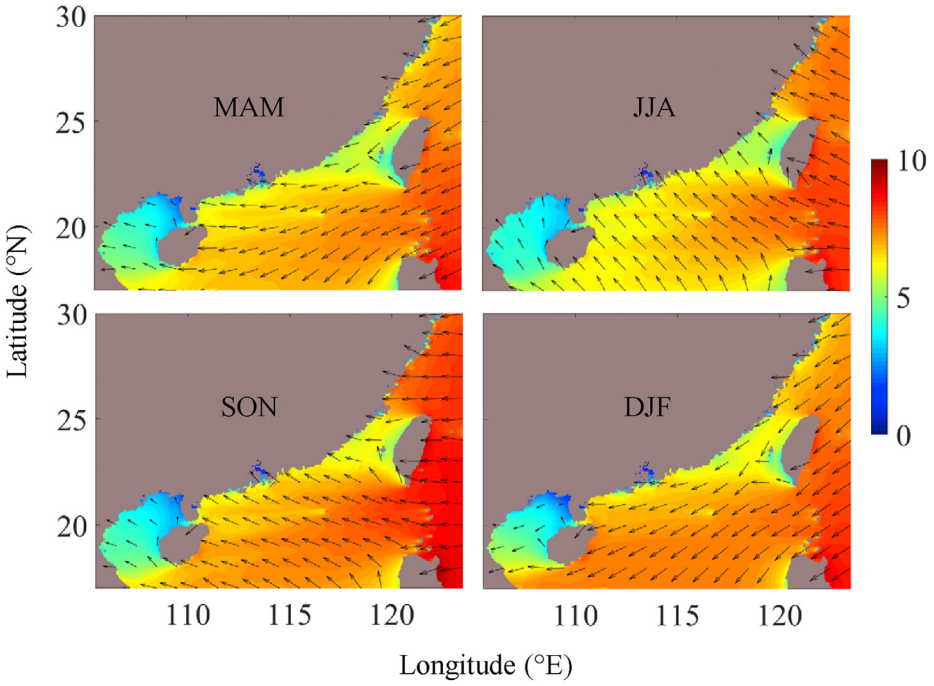

Fig. 8. 55-yearly seasonal T_e (s).

related to the operation and energy production of the wave farm, while H_{max} is representative of extreme sea states. Therefore, higher values of WEI indicate a greater ratio of mean to extreme wave heights and, *caeteris paribus,* greater suitability for wave energy extraction. The interest of the WEI index lies in that it is a metric specifically designed for assessing the suitability of a wave climate for its exploitation as an energy resource. Of course, other metrics are also relevant. In fact, it is recommended that the WEI index be used as part of a multi-criteria approach, alongside other parameters – importantly, parameters relating to mean wave power. One possibility in this respect would be to consider wave resource classes [26]. Another possibility is to use the SI_p. This is the approach adopted in this work.

Fig. 12 shows the mean annual wave power, RoC, MVI, SI_p, and WEI at 38 selected stations. According to this figure, offshore stations have higher mean annual wave power and higher RoC, while

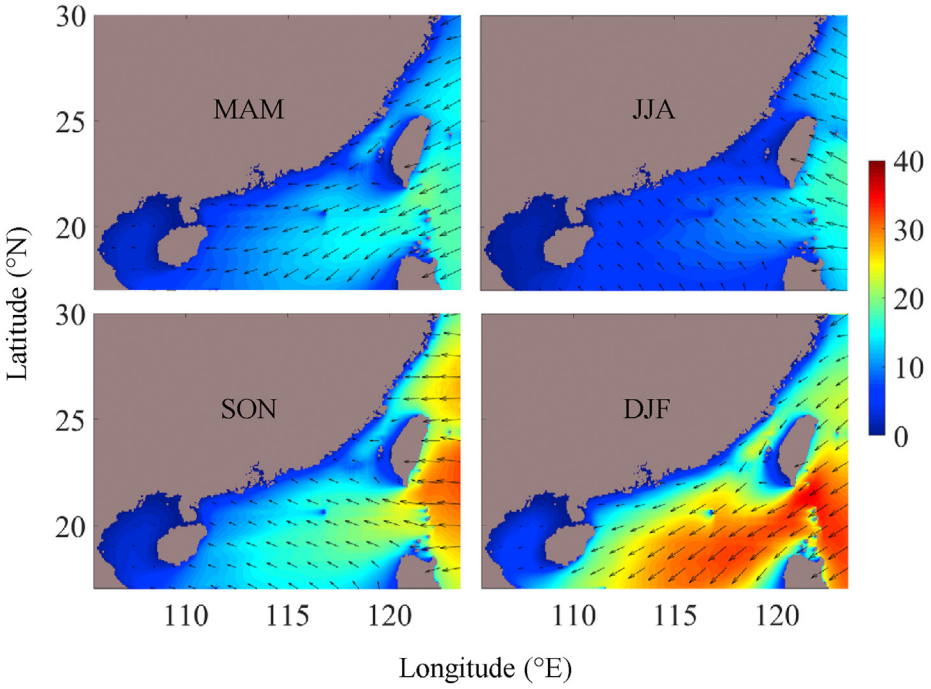

Fig. 9. 55-yearly seasonal mean P (kW/m).

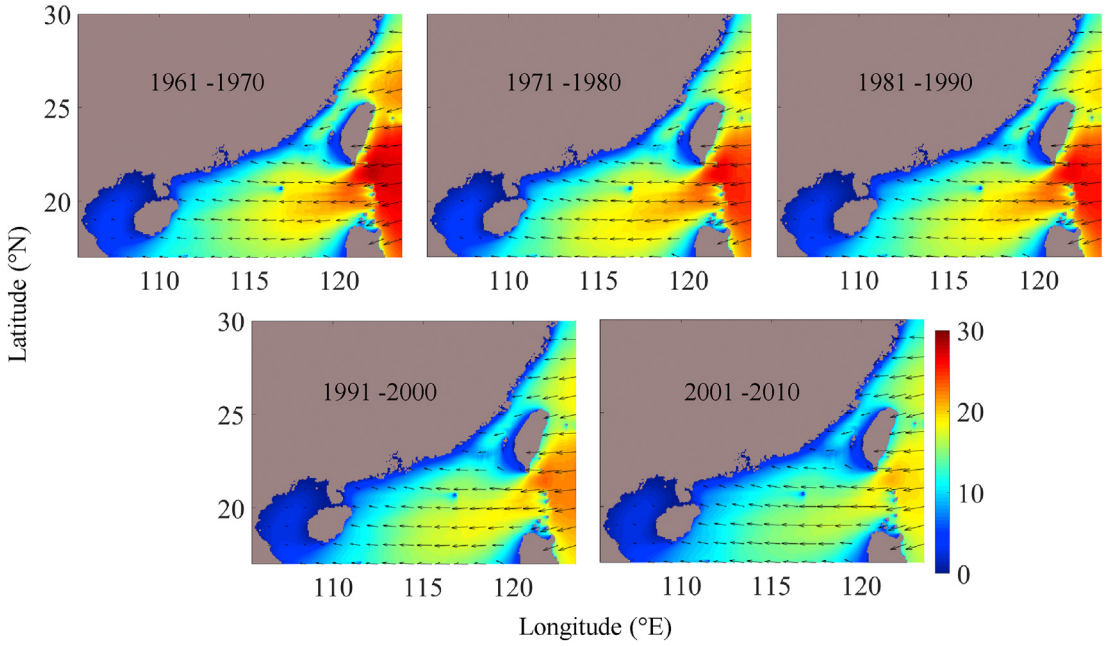

Fig. 10. 10-yearly annual mean P (kW/m).

both nearshore and offshore stations show a nearly similar range of MVI values.

The values shown in Fig. 12 indicate higher SI_p for offshore stations in comparison with their corresponding nearshore stations, which implies the priority of offshore stations compared to nearshore ones for selection of suitable locations. By contrast, relatively higher WEI values occur in nearshore stations, which is likely due to the extreme wave heights in the denominator of the WEI ratio being limited by depth-induced wave breaking.

According to the SI_p, the most suitable locations are: N6, N7, N11, N13, O12, O13, O18, and O19, while according to the WEI, the most suitable locations are: N6, N7, N9, N11, N13, N16, N17, N19, O12, O13, O16, O17, O18, and O19. On this basis, the following four stations nearshore and four stations offshore were selected for further assessment of suitable location and wave energy converter: N6, N7, N11, N13, O12, O13, O18, and O19.

3.4. Selection of suitable location/WEC

In this section, the combined selection of suitable locations and

Table 2
Selected stations and their characteristics.

Location	Station ID	Longitude (°E)	Latitude (°N)	Depth (d) (m)	Distance from coast (km)	Mean annual P (kW/m)	H_s (m)	T_m (s)	Wavelength (L) (m)	d/L
Nearshore	N1	110	20.9	3.75	3.2	0.13	0.24	1.94	5.87	0.64
	N2	109	19.8	8.5	1.2	0.53	0.35	2.54	10.00	0.85
	N3	109	19.1	8	2	0.45	0.38	2.46	9.44	0.85
	N4	109	18.5	5.5	2.9	0.52	0.41	3.06	14.58	0.38
	N5	110	18.2	20.4	2.5	3.46	0.92	4.63	33.40	0.61
	N6	110	18.7	18	1.6	5.49	1.04	6.12	56.40	0.32
	N7	111	19.7	20	1.15	7.03	1.21	5.73	50.60	0.40
	N8	111	20.2	6.5	1	1.27	0.55	4.58	29.00	0.22
	N9	111	20.9	8.75	2.4	2.41	0.77	4.80	33.40	0.26
	N10	112	21.5	9.5	1.9	1.83	0.69	4.51	30.40	0.31
	N11	113	21.9	13	2.1	2.62	0.82	4.62	32.90	0.40
	N12	114	22.4	11.5	2	2.80	0.83	4.95	36.70	0.31
	N13	116	22.7	13	1.6	3.22	0.91	4.62	32.80	0.40
	N14	116	22.9	6.75	3	2.18	0.74	4.59	29.40	0.23
	N15	118	23.7	12.2	1.4	1.88	0.70	4.52	31.40	0.39
	N16	119	24.9	9.75	2	3.00	0.85	4.47	30.20	0.32
	N17	120	25.9	6.5	3.3	3.08	0.85	4.95	32.50	0.20
	N18	121	27.4	6	1.7	2.73	0.78	5.44	36.00	0.17
	N19	122	29.8	16.9	0.33	5.09	1.06	5.11	40.30	0.42
Offshore	O1	109	20.7	20	48	0.73	0.48	2.62	10.67	1.87
	O2	109	20.1	54	47	1.68	0.63	3.00	14.06	3.84
	O3	108	19.1	39.5	49.2	2.40	0.77	3.51	19.25	2.05
	O4	109	18.1	55	45.5	2.77	0.87	4.22	27.78	1.98
	O5	110	18.1	56.8	7	4.32	1.02	4.84	36.59	1.55
	O6	110	18.6	57.2	12.8	7.52	1.24	5.97	55.67	1.03
	O7	111	19.6	56	19.5	8.84	1.37	5.58	48.59	1.15
	O8	111	20.5	30	49.8	5.93	1.17	5.10	40.64	0.74
	O9	111	20.9	30	48.3	5.07	1.11	5.02	39.26	0.76
	O10	112	21.1	40	48.8	5.77	1.19	4.98	38.71	1.03
	O11	113	21.5	45.5	49	7.50	1.33	5.18	41.88	1.09
	O12	115	21.9	55.2	47	7.85	1.36	5.36	44.82	1.23
	O13	116	22.3	57.7	46.5	7.82	1.38	5.19	42.07	1.37
	O14	117	22.6	46.2	49.5	7.36	1.34	5.16	41.50	1.11
	O15	118	23.6	29.2	47.5	7.05	1.26	4.89	37.34	0.78
	O16	119	24.6	58.2	41.7	9.66	1.48	4.86	36.84	1.58
	O17	120	25.8	41.5	49.4	10.28	1.54	5.44	46.24	0.90
	O18	121	27.2	36	46.6	10.07	1.50	5.76	51.68	0.70
	O19	123	29.5	46.5	46.1	11.76	1.61	5.80	52.42	0.89

technologies is done based on the methods suggested by Ref. [45] (i.e., Multi-Criteria Approach, also known as MCA factor) consisting of various properties of wave climate and WECs. The analysis was performed for the candidate stations, i.e., N6, N7, N11, N13, O12, O13, O18, and O19 chosen in the previous section, and the WECs considered for this analysis are indicated in Table 4. It should be noticed that based on the recommended installation depth of each device, its usage in various candidate stations can be limited. Hence, the right column in Table 4 shows the candidate stations where the WEC can be installed based on the water depth provided in Table 2.

Based on different parameters including exploitable storages of wave energy, accessibility and availability, energy production and its intra-annual variation, and extreme events, a modified MCA factor was utilized to detect the most appropriate WEC for each station and determine the most suitable combination of location/WEC. More details for each parameter are provided in the next subsections.

3.4.1. Total and exploitable storages of wave energy

The total and exploitable storages of wave energy per unit area (E_t and E_e, respectively) were calculated as follows, based on the mean annual P (P_{mean}), total hours all year round (t = 8760 h), and the theoretical exploitable time (t_e) corresponding to wave power greater than a threshold (set at 2 kW/m according to Refs. [23,52]).

$$E_t = P_{mean} \times t \quad (10)$$

$$E_e = P_{mean} \times t_e \quad (11)$$

Table 5 shows t_e, E_e, E_t, and the ratio of E_e to E_t, indicating the highest exploitable storage of energy in O19 which contains the highest percentage in total storage (97.8%). In general, the exploitable storage of energy decreases from western to eastern stations. However, as well as the lowest total storage and exploitable storage, N11 and N13 contain the lowest ratios of E_e to E_t among the other stations.

3.4.2. Accessibility and availability

In order to consider the wave climate for operational and maintenance (O&M) purposes, "accessibility" has been defined to recognize the time slots when a safe sea condition is suitable for deployments of crews and vessels, and is calculated based on the percentage of the time when the wave height in a location is equal or less than a specific threshold [53]. In order to define when the resource favors WEC operation, "availability" is used as the percentage of time when the sea state is between WECs' cut-in ($H_{cut\text{-}in}$) and cut-off ($H_{cut\text{-}off}$) conditions. A range of 0.5 and 4 m has been considered for $H_{cut\text{-}in}$ and $H_{cut\text{-}off}$, respectively, according to Ref. [53]. Accessibility and availability calculated for candidate stations are shown in Table 6. According to this table, availability is higher than 90% in all stations, except for N11, where the wave

Fig. 11. Location of nearshore stations (Source: Google Earth, U.S. Dept. of State Geographer, © 2020 Google, © 2020 GeoBasis-DE/BKG, Data SIO, NOAA, U.S. Navy, NGA, GEBCO).

heights are less than 1.5 m in more than 96% of the time (accessibility). Considering the accessibility, the wave height is less than 2.5 m in more than 90% of the time and less than 2 m in more than 80% of the time in all stations. The station with the least accessibility when the wave heights are lower than 1.5 m is O19 (56.51%).

3.4.3. Energy production (E_0)

The energy production (E_0) is obtained based on both wave climate and properties of WECs, and is calculated as:

$$E_0 = \sum_{i=1}^{n_T} \sum_{j=1}^{n_H} p_{ij} P_{ij} \quad (12)$$

in which, p_{ij} is the percentage of occurrences of each sea state defined by H_s and T_e or T_p, and P_{ij} represents the electrical power yield provided by each WEC for the same energy bin [54,55]. The power matrices for different types of WECs used in this study can be found in Ref. [45]. Fig. 13 shows the energy production for different WECs at candidate stations, in which, Wave Dragon represents the highest E_0 in all stations. Considering Wave Dragon, O19 (located in the eastern coasts) has the highest energy production (~92000 MWh) among the offshore stations, while in nearshore, N7 (located in the northeast of Hainan) demonstrates the highest E_0 (~58000 MWh). The second highest energy production is provided by Wavestar C6 in nearshore stations. However, the values of E_0 by Wavestar C6 are considerably lower than those of Wave Dragon (less than half in nearshore stations). The lowest energy production

in all stations is obtained by to CECO. N11 and N13 are the stations with the lowest energy production in general.

Moreover, as well as the annual values, the stability of energy production on a monthly scale is important for purposes such as comparison with energy consumption and its seasonality, etc. The monthly variation of E_0 has been depicted in Figs. 14 and 15 for nearshore and offshore candidate stations, respectively. According to Fig. 14, the energy production in N6 and N7 is considerably higher than N11 and N13, especially during November and December, when E_0 is higher than 100,000 MWh for Wave Dragon. However, the monthly variations seem larger in N6 and N7. The energy production is the highest during November in all nearshore stations.

In offshore candidate stations (Fig. 15), Wave Dragon generates the highest energy production amongst the other types of WEC, with the highest values during November in O12 and O13, October in O18, and September and August in O19. This shows that the intra-annual variation of energy production varies with location.

In order to quantify the monthly variability, MVI was obtained for E_0. Fig. 16 depicts the MVI values for energy production. Offshore candidate stations, despite having the highest E_0 (for Wave Dragon), show lower intra-annual variability and hence, higher stability. Comparison of stations with higher and lower energy production in both nearshore and offshore (Figs. 13 and 16) indicates that in offshore, the stations with higher energy production (O18 and O19) are slightly more stable in terms of monthly variation of the resources. However, in nearshore stations, the stations with higher energy production (N6 and N7) present higher monthly variabilities. Hence, according to the wave climate at the candidate stations in this study, the monthly variability is directly and inversely proportional to energy production in nearshore and offshore stations, respectively.

3.4.4. Extreme events

In the methodology introduced by Ref. [45], the design wave height has been considered a representative of the design cost. In this study, in order to avoid the impact of utilized distribution on the results of the extreme value analysis, 99th and 95th percentiles of H_s were considered. As shown in Fig. 17, the extreme events in N7 are comparable to those of offshore stations, while the wave climate is the calmest in N11 and N13. In addition, the difference between 99th and 95th percentiles slightly increases in O18 and O19 implying the higher frequency of extreme events in eastern parts of the domain.

3.4.5. Multi-criteria approach (MCA)

The previous MCA factor developed by Ref. [45] utilizes constants based on the amount of the variables in the study area where it was applied. However, modifications were required in order to generalize it for other wave climates. For this purpose, the constant values proposed by Ref. [45] were replaced by the maximum (max) or minimum (min) values of each parameter across all considered stations. Hence, the MCA factor developed by Ref. [45] was modified as Eq. (13) and calculated based on the information of candidate stations and selected WECs as explained in the previous subsections. A higher MCA value shows more suitability for a combination of location/WEC.

$$MCA = \left(\frac{\frac{E_e}{max(E_e)} \times accessibility_{(H_s<1.5)} \times availability \times \frac{E_0}{max(E_0)} \times \frac{min(H_s\ 99th\ percentile)}{H_s\ 99th\ percentile}}{MVI_{E_0}} \right. \tag{13}$$

Fig. 18 illustrates the modified MCA factor for different combinations of stations and WECs. It shows that the most suitable combination of location/WEC in offshore is Wave Dragon in O19. Investigating MCA in each station, individually indicates that the most suitable WECs are Wave Dragon in O12, O13, O18, and O19, and OWC in all nearshore candidate stations. Comparing the suitability of each WEC for offshore stations demonstrates that all WECs are more appropriate if they are deployed in O19. In nearshore stations, nearshore WECs are more appropriate if they are deployed in N7, except for OWC, which is more appropriate to be installed in N13. Hence, if a priority location/WEC should be decided for the installation of wave farms, Wave Dragon in O19 and O18 could be the proper option. However, if multiple locations are going to be considered for the installation of wave farms with one type of WEC as a priority, OWC and Wave Dragon could be the most appropriate choices for nearshore and offshore stations, respectively.

Table 3
Relative error for calulation of wave power based on deep water approximation.

Station ID	n	C	E	P_{tr} (kW/m) = Ecn	P (kW/m)	Error (kW/m)
N4	0.54	4.77	0.10	0.267	0.253	−0.014
N6	0.57	9.22	0.67	3.514	3.255	−0.259
N7	0.53	8.82	0.90	4.223	4.103	−0.120
N8	0.67	6.33	0.18	0.772	0.667	−0.105
N9	0.62	6.96	0.36	1.565	1.387	−0.178
N10	0.58	6.74	0.29	1.128	1.044	−0.085
N11	0.53	7.12	0.41	1.561	1.516	−0.045
N12	0.58	7.41	0.42	1.788	1.656	−0.132
N13	0.53	7.10	0.51	1.928	1.874	−0.054
N14	0.66	6.40	0.34	1.420	1.231	−0.189
N15	0.54	6.95	0.30	1.127	1.091	−0.036
N16	0.57	6.75	0.45	1.715	1.594	−0.122
N17	0.70	6.56	0.45	2.066	1.768	−0.297
N18	0.76	6.62	0.37	1.871	1.613	−0.258
N19	0.53	7.89	0.69	2.885	2.834	−0.051

4. Summary and conclusion

In this study, the potential areas in the south of China were investigated for wave energy extraction. For this purpose, high-resolution wave modeling was carried out to generate the wave characteristics for 55 years. The model was validated against the buoy dataset for different periods and, subsequently, run to generate the wave climate in the long-term. The intra-annual variation of wave climate and wave energy resources showed that the wave energy is greatest in the eastern parts of the domain. However, the effect of seasonality on wave energy and wave propagation direction cannot be neglected there. Moreover, the long-term availability of wave climate provided the opportunity to evaluate the resources in various time spans. The decadal mean of wave power in the whole domain showed that it has decreased in

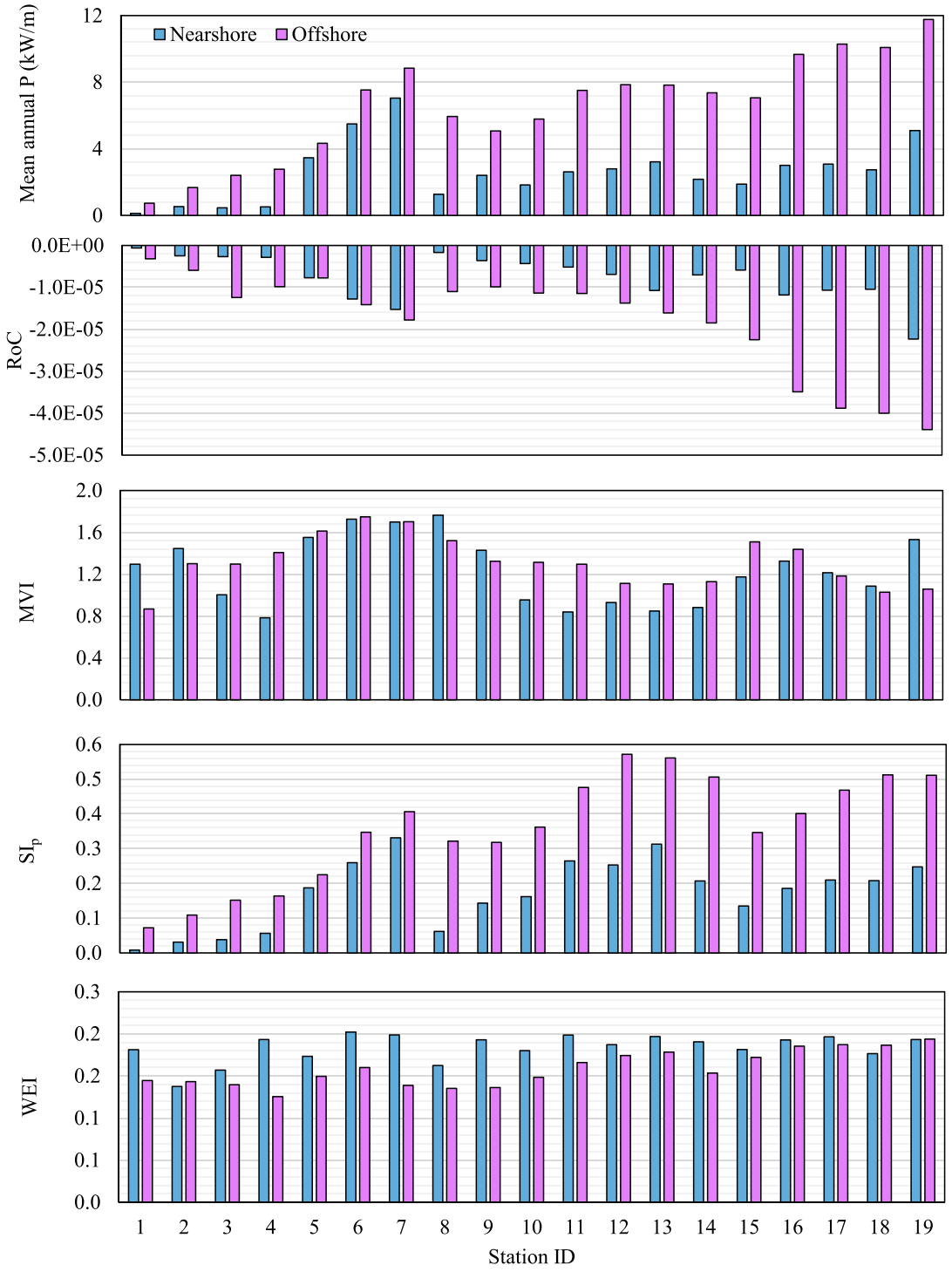

Fig. 12. Different parameters in selected stations.

recent decades, especially in the areas with higher potential (east of domain), while the wave energy has been relatively stable in the northern parts of the domain (southern coasts of China). Hence, it is important to consider the assessment period long enough to include the decadal variation and select the right time span for the analysis.

For quantitative assessment, 38 stations were selected in nearshore and offshore by specified criteria, and a combined approach involving two indices (SI_p and WEI) was applied to the selection of the most suitable ones among them. As a ratio between mean and extreme wave heights, the WEI index reflects primarily stability (or inverse variability) in the wave resource, and should be combined in the approach with a wave power estimator – hence the rationale of combining the WEI and SI_p. The SI_p values are higher for offshore stations, while the WEI values are slightly higher for nearshore stations (due to the reduction in the extreme wave heights as a result of depth-induced wave breaking). Importantly for the combined approach, the comparison between nearshore and offshore

Table 4
Main characteristics of selected WECs.

Technology	Rated power (kW)	Classification	Matrix resolution ($H_s \times T_e$ or T_p)	Installation depth (m)	Candidate stations
OWC [46]	85	Terminator	1.0 m × 1.1 s	<20	N6, N7, N11, and N13
Oyster [47]	290	Terminator	0.5 m × 1.0 s	10–25	N6, N7, N11, and N13
Wavestar C6 [48]	600	Point absorber	0.5 m × 1.0 s	10–30	N6, N7, N11, and N13
OEbuoy [49]	2880	Oscillating water column	0.5 m × 1.0 s	Around 20	N6, N7, N11, and N13
CECO [50]	692	Point absorber	1.0 m × 2.0 s	20–50	N6, N7, O18, and O19
Wave Dragon [46]	6000	Terminator	0.5 m × 0.5 s	>20	N6, N7, O12, O13, O18, and O19
Langlee [50]	1665	Oscillating wave surge	0.5 m × 1.0 s	>10	All
Archimedes [46,51]	2500	Point absorber	0.5 m × 0.5 s	>50	O12, O13, and O19
WaveBob [50]	1000	Point absorber	0.5 m × 0.5 s	>50	O12, O13, and O19
Aquabuoy [47,50]	250	Point absorber	0.5 m × 1.0 s	50–60	O12, O13, and O19

Table 5
E_e and E_t in candidate stations.

Station ID	t_e (hr)	E_e (kWh/m)	E_t (kWh/m)	E_e/E_t (%)
N6	5380	29,550.6	48,111.5	61.4
N7	6039	42,521.3	61,685.2	68.9
N11	3359	8814.4	22,987.8	38.3
N13	4168	13,422.6	28,207.5	47.6
O12	7289	57,247.3	68,802.3	83.2
O13	6987	54,653.2	68,521.3	79.8
O18	8511	85,755.9	88,265.4	97.2
O19	8564	100,694.6	103,003.5	97.8

stations showed that both factors lead to selecting similar stations as the most suitable. On this basis, eight stations (four nearshore and four offshore) were selected as candidate stations for further assessment and selection of suitable WEC.

The analysis on the next level was based on the modified MCA factor, which has been defined considering both wave climate and WEC properties. The components of the MCA factor, including exploitable storage of wave energy, accessibility, availability, energy production, and its intra-annual variation, and extreme events were assessed and the suitability of candidate stations and WECs were discussed. Then, the combined suitability of location/WEC was determined with the use of the MCA factor.

The results showed that Wave Dragon is the best choice in all offshore stations. However, if the target is to install the wave farms nearshore, OWC is the most appropriate WEC. In addition, for all the types of WECs considered, stations O19 and N7 are the most appropriate locations in offshore and nearshore, respectively, except for OWC which outperforms in N13. If the installation of wave farms is planned at various locations with only one type of WEC, then Wave Dragon and OWC are recommended for offshore

Table 6
Accessibility and availability at candidate stations.

	Accessibility							Availability
	Hs < 1.5	Hs < 2	Hs < 2.5	Hs < 3	Hs < 3.5	Hs < 4	Hs < 4.5	0.5<Hs < 4
N6	84.55	94.91	98.51	99.51	99.78	99.87	99.92	97.60
N7	75.04	89.15	96.03	98.61	99.46	99.72	99.84	98.16
N11	96.39	98.93	99.55	99.76	99.86	99.91	99.96	88.37
N13	93.96	98.38	99.33	99.64	99.79	99.89	99.94	94.43
O12	66.62	85.50	94.91	98.18	99.20	99.57	99.75	99.32
O13	65.33	83.81	93.77	97.69	99.06	99.52	99.72	99.21
O18	61.43	82.99	92.98	97.15	98.62	99.21	99.48	98.87
O19	56.51	79.50	89.96	95.04	97.58	98.74	99.26	98.46

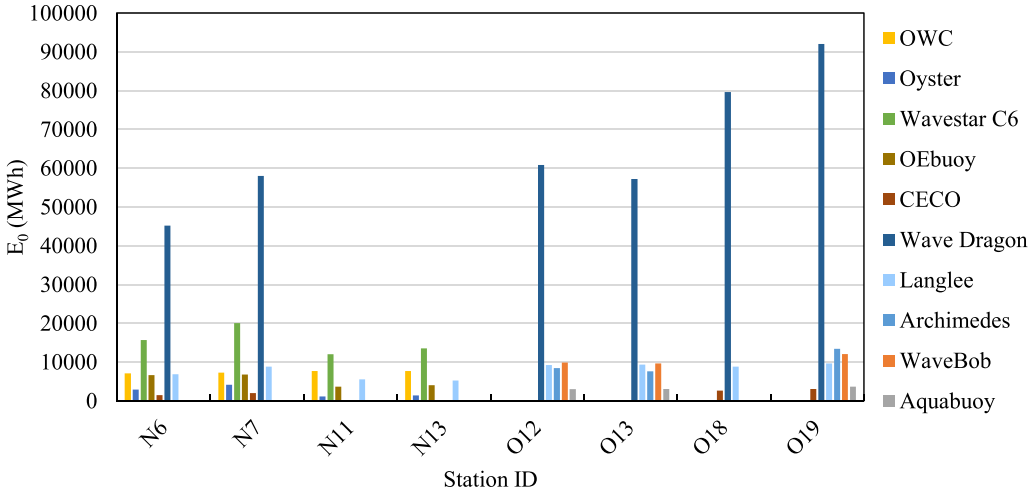

Fig. 13. Annual E_0 (MWh) values for candidate stations.

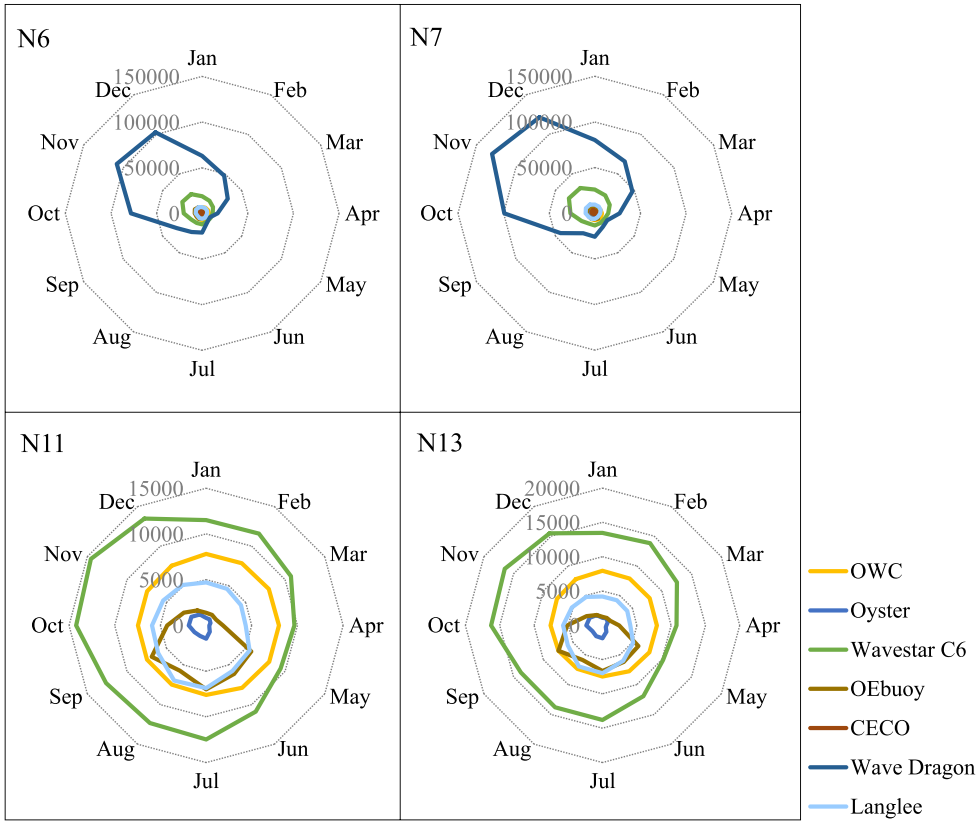

Fig. 14. Monthly E_0 (MWh) values for nearshore candidate stations.

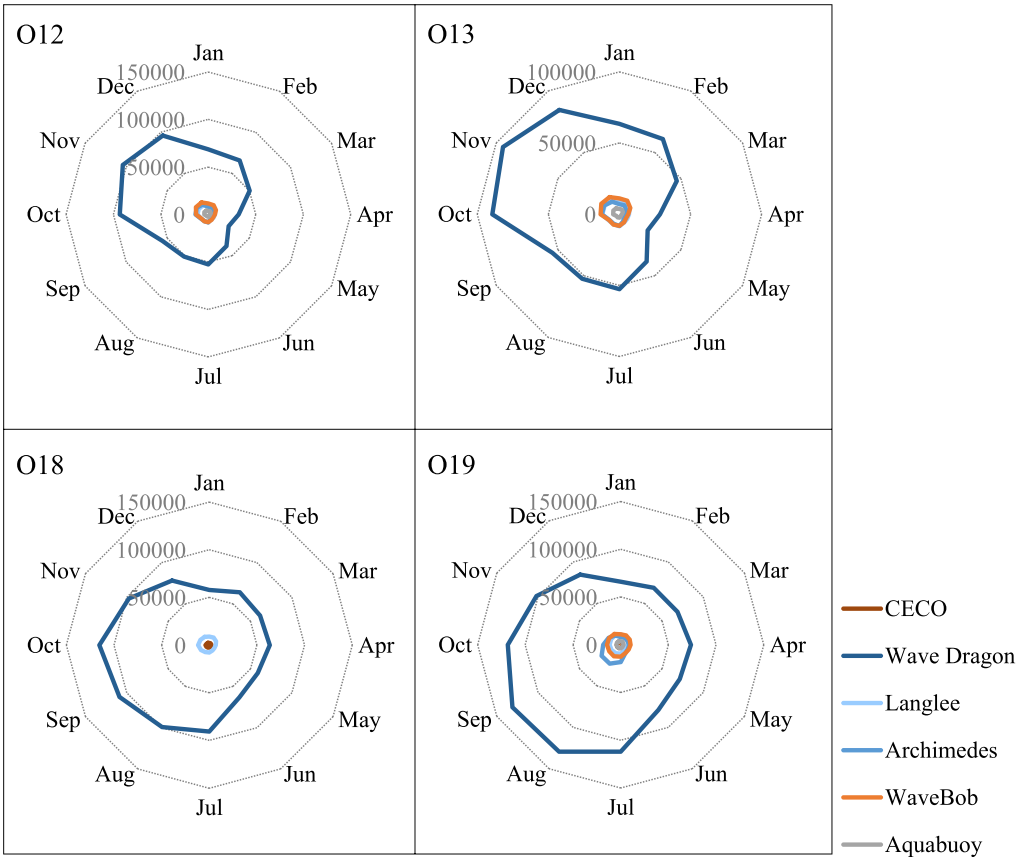

Fig. 15. Monthly E_0 (MWh) values for offshore candidate stations.

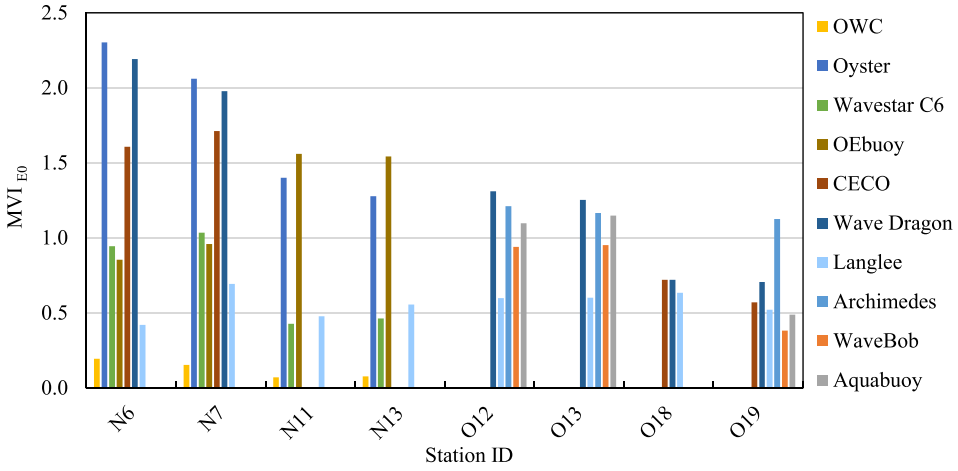

Fig. 16. MVI $_{E0}$ for candidate stations.

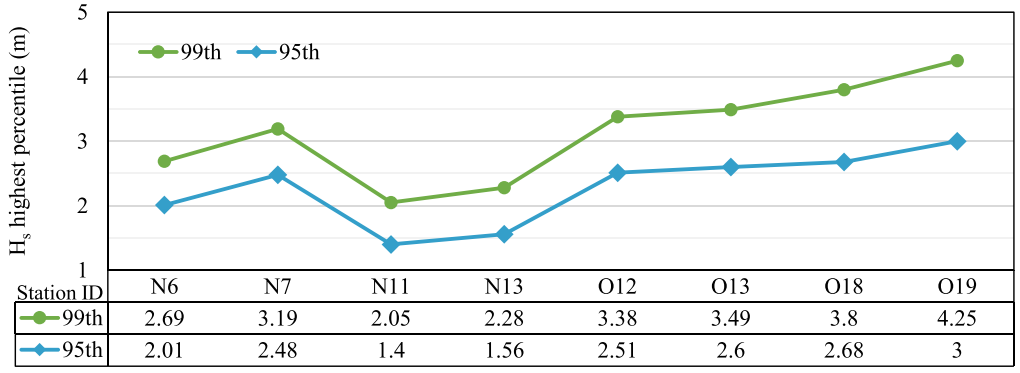

Station ID	N6	N7	N11	N13	O12	O13	O18	O19
99th	2.69	3.19	2.05	2.28	3.38	3.49	3.8	4.25
95th	2.01	2.48	1.4	1.56	2.51	2.6	2.68	3

Fig. 17. H_s highest percentile for candidate stations.

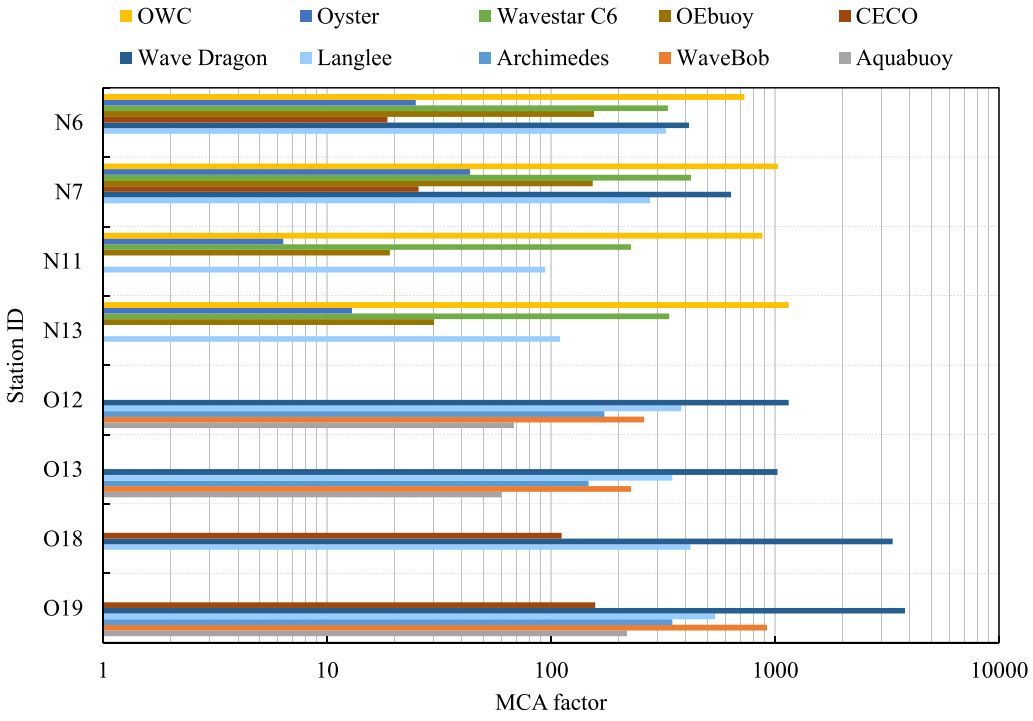

Fig. 18. MCA factor values for offshore candidate stations.

and nearshore, respectively, based on the results of this research.

Using the developed methodology, the results of this research provides the required information for decision-maker based on wave climate in both short and long-term and the available technical specifications of the devices. However, further economic assessments are necessary to estimate the final cost and provide additional information for future planning.

Declaration of competing interest

The authors declare that they have no known competing financial interests or personal relationships that could have appeared to influence the work reported in this paper.

Acknowledgement

This research has been conducted under the grant No. Skhl1807 supported by State Key Laboratory of Hydraulics and Mountain River Engineering, Sichuan University, and the grant from NSFC (51879237). Part of this work has been supported by the Hakubi Center for Advanced Research at Kyoto University, and JSPS Grants-in-Aid for Scientific Research (KAKENHI), grant No. 20K04705, supported by the Ministry of Education, Culture, Sports, Science, and Technology of Japan (MEXT). The authors are thankful to Japan Meteorological Agency (JMA) for providing JRA-55 dataset, to the SWAN team at Delft University of Technology for making the model freely available, and to MaREI (Science Foundation Ireland) for their support. The authors also thank the editor and two anonymous reviewers for their fruitful comments.

References

[1] S. Shafiee, E. Topal, When will fossil fuel reserves be diminished? Energy Pol. 37 (2009) 181–189, https://doi.org/10.1016/j.enpol.2008.08.016.
[2] IEA Renewables 2020 Analysis and Forecast to 2025, 2020.
[3] C.W. Zheng, Q. Wang, C.Y. Li, An overview of medium- to long-term predictions of global wave energy resources, Renew. Sustain. Energy Rev. 79 (2017) 1492–1502, https://doi.org/10.1016/j.rser.2017.05.109.
[4] A. Pecher, J.P. Kofoed (Eds.), Handbook of Ocean Wave Energy, Springer International Publishing, 2017, https://doi.org/10.1007/978-3-319-39889-1.
[5] C. Rodriguez-Delgado, R.J. Bergillos, G. Iglesias, Dual wave farms and coastline dynamics: the role of inter-device spacing, Sci. Total Environ. 646 (2019) 1241–1252, https://doi.org/10.1016/j.scitotenv.2018.07.110.
[6] C. Rodriguez-Delgado, R.J. Bergillos, G. Iglesias, Dual wave farms for energy production and coastal protection under sea level rise, J. Clean. Prod. 222 (2019) 364–372, https://doi.org/10.1016/j.jclepro.2019.03.058.
[7] Y. Lin, S. Dong, Z. Wang, C. Guedes Soares, Wave energy assessment in the China adjacent seas on the basis of a 20-year SWAN simulation with unstructured grids, Renew. Energy 136 (2019) 275–295, https://doi.org/10.1016/j.renene.2019.01.011.
[8] S. Wu, C. Liu, X. Chen, Offshore wave energy resource assessment in the East China Sea, Renew. Energy 76 (2015) 628–636, https://doi.org/10.1016/j.renene.2014.11.054.
[9] G. Zhou, J. Huang, G. Zhang, Evaluation of the wave energy conditions along the coastal waters of Beibu Gulf, China, Energy 85 (2015) 449–457, https://doi.org/10.1016/j.energy.2015.03.094.
[10] Q. Liu, K.D. Koper, R. Burlacu, S. Ni, F. Wang, C. Zou, Y. Wei, M. Gal, A.M. Reading, Source locations of teleseismic P, SV, and SH waves observed in microseisms recorded by a large aperture seismic array in China, Earth Planet Sci. Lett. 449 (2016) 39–47, https://doi.org/10.1016/j.epsl.2016.05.035.
[11] A. Mirzaei, F. Tangang, L. Juneng, Wave energy potential assessment in the central and southern regions of the South China Sea, Renew. Energy 80 (2015) 454–470, https://doi.org/10.1016/j.renene.2015.02.005.
[12] C.W. Zheng, C.Y. Li, Variation of the wave energy and significant wave height in the China Sea and adjacent waters, Renew. Sustain. Energy Rev. 43 (2015) 381–387, https://doi.org/10.1016/j.rser.2014.11.001.
[13] B. Liang, F. Fan, Z. Yin, H. Shi, D. Lee, Numerical modelling of the nearshore wave energy resources of Shandong peninsula, China, Renew. Energy 57 (2013) 330–338, https://doi.org/10.1016/j.renene.2013.01.052.
[14] G. Zhou, J. Huang, T. Yue, Q. Luo, G. Zhang, Temporal-spatial distribution of wave energy: a case study of Beibu Gulf, China, Renew. Energy 74 (2015) 344–356.
[15] Z. Sun, H. Zhang, D. Xu, X. Liu, J. Ding, Assessment of wave power in the South China Sea based on 26-year high-resolution hindcast data, Energy 197 (2020) 117218, https://doi.org/10.1016/j.energy.2020.117218.
[16] S. Dong, Y. Gong, Z. Wang, A. Incecik, Wind and wave energy resources assessment around the Yangtze River Delta, Ocean. Eng. 182 (2019) 75–89, https://doi.org/10.1016/j.oceaneng.2019.04.030.
[17] D. Zhang, W. Li, Y. Lin, Wave energy in China: current status and perspectives, Renew. Energy 34 (2009) 2089–2092, https://doi.org/10.1016/j.renene.2009.03.014.
[18] Y. Zhang, Z. Lin, Q. Liu, Marine renewable energy in China: current status and perspectives, Water Sci. Eng. 7 (2014) 288–305, https://doi.org/10.3882/j.issn.1674-2370.2014.03.005.
[19] Y. Liu, Y. Li, F. He, H. Wang, Comparison study of tidal stream and wave energy technology development between China and some Western Countries, Renew. Sustain. Energy Rev. 76 (2017) 701–716, https://doi.org/10.1016/j.rser.2017.03.049.
[20] Y. Wan, C. Zheng, L. Li, Y. Dai, M.D. Esteban, J.-S. López-Gutiérrez, X. Qu, X. Zhang, Wave energy assessment related to wave energy convertors in the coastal waters of China, Energy 202 (2020) 117741, https://doi.org/10.1016/j.energy.2020.117741.
[21] S. Qiu, K. Liu, D. Wang, J. Ye, F. Liang, A comprehensive review of ocean wave energy research and development in China, Renew. Sustain. Energy Rev. 113 (2019) 109271, https://doi.org/10.1016/j.rser.2019.109271.
[22] Z. Wang, C. Duan, S. Dong, Long-term wind and wave energy resource assessment in the South China sea based on 30-year hindcast data, Ocean. Eng. 163 (2018) 58–75, https://doi.org/10.1016/j.oceaneng.2018.05.070.
[23] C. Zheng, J. Pan, J. Li, Assessing the China Sea wind energy and wave energy resources from 1988 to 2009, Ocean. Eng. 65 (2013) 39–48, https://doi.org/10.1016/j.oceaneng.2013.03.006.
[24] X. Chen, K. Wang, Z. Zhang, Y. Zeng, Y. Zhang, K. O'Driscoll, An assessment of wind and wave climate as potential sources of renewable energy in the nearshore Shenzhen coastal zone of the South China Sea, Energy 134 (2017) 789–801, https://doi.org/10.1016/j.energy.2017.06.043.
[25] B. Kamranzad, G. Lavidas, K. Takara, Spatio-temporal assessment of climate change impact on wave energy resources using various time dependent criteria, Energies 13 (2020) 768, https://doi.org/10.3390/en13030768.
[26] A. Martinez, G. Iglesias, Wave exploitability index and wave resource classification, Renew. Sustain. Energy Rev. 134 (2020) 110393, https://doi.org/10.1016/j.rser.2020.110393.
[27] G. Lavidas, B. Kamranzad, Assessment of wave power stability and classification with two global datasets, Int. J. Sustain. Energy (2020) 1–16, https://doi.org/10.1080/14786451.2020.1821027.
[28] B. Kamranzad, A. Etemad-Shahidi, V. Chegini, A. Yeganeh-Bakhtiary, Climate change impact on wave energy in the Persian Gulf, Ocean Dynam. 65 (2015) 777–794, https://doi.org/10.1007/s10236-015-0833-y.
[29] H. Karunarathna, P. Maduwantha, B. Kamranzad, H. Rathnasooriya, K. [de Silva], Evaluation of spatio-temporal variability of ocean wave power resource around Sri Lanka, Energy 200 (2020) 117503, https://doi.org/10.1016/j.energy.2020.117503.
[30] B. Bingölbali, H. Jafali, A. Akpınar, S. Bekiroğlu, Wave energy potential and variability for the south west coasts of the Black Sea: the WEB-based wave energy atlas, Renew. Energy 154 (2020) 136–150, https://doi.org/10.1016/j.renene.2020.03.014.
[31] S. Ahn, V.S. Neary, Non-stationary historical trends in wave energy climate for coastal waters of the United States, Ocean. Eng. 216 (2020) 108044, https://doi.org/10.1016/j.oceaneng.2020.108044.
[32] L. Rusu, Evaluation of the near future wave energy resources in the Black Sea under two climate scenarios, Renew. Energy 142 (2019) 137–146, https://doi.org/10.1016/j.renene.2019.04.092.
[33] L. Rusu, A projection of the expected wave power in the Black Sea until the end of the 21st century, Renew. Energy 160 (2020) 136–147, https://doi.org/10.1016/j.renene.2020.06.092.
[34] M.V.W. Cuttler, J.E. Hansen, R.J. Lowe, Seasonal and interannual variability of the wave climate at a wave energy hotspot off the southwestern coast of Australia, Renew. Energy 146 (2020) 2337–2350, https://doi.org/10.1016/j.renene.2019.08.058.
[35] I. López, R. Carballo, G. Iglesias, Intra-annual variability in the performance of an oscillating water column wave energy converter, Energy Convers. Manag. 207 (2020) 112536, https://doi.org/10.1016/j.enconman.2020.112536.
[36] B. Kamranzad, P. Lin, Sustainability of wave energy resources in the South China Sea based on five decades of changing climate, Energy 210 (2020) 118604, https://doi.org/10.1016/j.energy.2020.118604.
[37] G. Lavidas, Selection index for Wave Energy Deployments (SIWED): a near-deterministic index for wave energy converters, Energy 196 (2020) 117131, https://doi.org/10.1016/j.energy.2020.11713.
[38] J. Zhou, Z. Wu, D. Zhao, W. Guan, C. Zhu, B. Flemming, Giant sand waves on the Taiwan Banks, southern Taiwan Strait: distribution, morphometric relationships, and hydrologic influence factors in a tide-dominated environment, Mar. Geol. 427 (2020) 106238, https://doi.org/10.1016/j.margeo.2020.106238.
[39] J. Zhou, Z. Wu, X. Jin, D. Zhao, Z. Cao, W. Guan, Observations and analysis of giant sand wave fields on the Taiwan Banks, northern South China Sea, Mar. Geol. 406 (2018) 132–141, https://doi.org/10.1016/j.margeo.2018.09.015.
[40] N. Booij, R.C. Ris, L.H. Holthuijsen, A third-generation wave model for coastal regions: 1. Model description and validation, J. Geophys. Res. Ocean. 104 (1999) 7649–7666, https://doi.org/10.1029/98JC02622.
[41] S. Kobayashi, Y. Ota, Y. Harada, A. Ebita, M. Moriya, H. Onoda, K. Onogi, H. Kamahori, C. Kobayashi, H. Endo, K. Miyaoka, K. Takahashi, The JRA-55 reanalysis: general specifications and basic characteristics, J. Meteorol. Soc.

Japan. Ser. II. 93 (2015) 5–48, https://doi.org/10.2151/jmsj.2015-001.
[42] R.M. Sorensen, Basic Coastal Engineering, 3rd ed., Springer US, 2006, https://doi.org/10.1007/b101261.
[43] B. Kamranzad, K. Takara, A climate-dependent sustainability index for wave energy resources in Northeast Asia, Energy 209 (2020) 118466, https://doi.org/10.1016/j.energy.2020.118466.
[44] A.M. Cornett, A global wave energy resource assessment, in: Proc. Int. Offshore Polar Eng. Conf., 2008, pp. 318–326. https://www.scopus.com/inward/record.uri?eid=2-s2.0-58449099012&partnerID=40&md5=22704af189c0a8b72388d30e50169234.
[45] B. Kamranzad, S. Hadadpour, A multi-criteria approach for selection of wave energy converter/location, Energy 204 (2020) 117924, https://doi.org/10.1016/j.energy.2020.117924.
[46] M. Veigas, M. López, P. Romillo, R. Carballo, A. Castro, G. Iglesias, A proposed wave farm on the Galician coast, Energy Convers. Manag. 99 (2015) 102–111, https://doi.org/10.1016/j.enconman.2015.04.033.
[47] D. Silva, E. Rusu, C.G. Soares, Evaluation of various technologies for wave energy conversion in the Portuguese nearshore, Energies 6 (2013), https://doi.org/10.3390/en6031344.
[48] L. Marquis, M. Kramer, J. Kringelum, J.F. Chozas, N.E. Helstrup, Introduction of wavestar wave energy converters at the Danish offshore wind power, Plant Horns Rev 2 (2012).
[49] Testing of ocean energy buoy at galway bay, Ireland, (n.d.). https://tethys.pnnl.gov/project-sites/testing-ocean-energy-buoy-galway-bay-ireland.
[50] A. Babarit, J. Hals, M.J. Muliawan, A. Kurniawan, T. Moan, J. Krokstad, Numerical benchmarking study of a selection of wave energy converters, Renew. Energy 41 (2012) 44–63, https://doi.org/10.1016/j.renene.2011.10.002.
[51] D. Valério, P. Beirão, J. Sá da Costa, Optimisation of wave energy extraction with the archimedes wave swing, Ocean. Eng. 34 (2007) 2330–2344, https://doi.org/10.1016/j.oceaneng.2007.05.009.
[52] B. Wen, Y.G. Xue, F.R. Zhang, C.Y. Zhao, Numerical simulation of wave energy resources in the China Sea, Mar. Forecasts 30 (2013) 36–41.
[53] G. Lavidas, A. Agarwal, V. Venugopal, Availability and accessibility for offshore operations in the mediterranean sea, J. Waterw. Port, Coast. Ocean Eng. 144 (2018), 05018006.
[54] J. Morim, N. Cartwright, M. Hemer, A. Etemad-Shahidi, D. Strauss, Inter- and intra-annual variability of potential power production from wave energy converters, Energy 169 (2019) 1224–1241, https://doi.org/10.1016/j.energy.2018.12.080.
[55] R. Carballo, M. Sánchez, V. Ramos, A. Castro, A tool for combined WEC-site selection throughout a coastal region: rias Baixas, NW Spain, Appl. Energy 135 (2014) 11–19, https://doi.org/10.1016/j.apenergy.2014.08.068.